Role of nonlinear effects in nanowire growth and crystal phase

V. G. Dubrovskii,[1,2,*] N. V. Sibirev,[1] G. E. Cirlin,[1,2,3] A. D. Bouravleuv,[1,2] Yu. B. Samsonenko,[1,2] D. L. Dheeraj,[4] H. L. Zhou,[4] C. Sartel,[3] J. C. Harmand,[3] G. Patriarche,[3] and F. Glas[3]

[1]*St. Petersburg Physics and Technology Centre for Research and Education, Russian Academy of Sciences, Khlopina 8/3, 195220 St. Petersburg, Russia*

[2]*Ioffe Physical-Technical Institute of the Russian Academy of Sciences, Politekhnicheskaya 26, 194021 St. Petersburg, Russia*

[3]*CNRS–LPN, Route de Nozay, 91460 Marcoussis, France*

[4]*Department of Electronics and Telecommunications, Norwegian University of Science and Technology, NO-7491 Trondheim, Norway*

(Received 28 April 2009; revised manuscript received 29 June 2009; published 6 November 2009)

We study theoretically and experimentally nonlinear effects during the "vapor-liquid-solid" growth of semiconductor nanowires. Nonlinear growth equation considered contains kinetic coefficients from the surface and sidewall diffusion which can be of either signs. We predict four possible growth scenarios: (I) infinite growth; (II) decomposition; (III) averaging growth to a finite length; and (IV) continuing growth such that nanowires of small initial length decay and longer nanowires grow infinitely. We present the experimental evidence of nontrivial scenarios (II) and (IV) during the Au-assisted molecular-beam epitaxy of GaAs nanowires. Scenario (II) corresponds to the evaporation of GaAs nanowires during the annealing. Scenario (IV) is observed during two-step growth procedure where a low-temperature growth is followed by deposition at 630 °C. We show that the growth via scenario (IV) enables to control the crystal phase and to obtain the stacking-fault-free sections of zinc-blende GaAs NWs having only 15–20 nm in radius.

DOI: 10.1103/PhysRevB.80.205305 PACS number(s): 81.10.Aj, 68.70.+w

I. INTRODUCTION

Free-standing semiconductor nanowires (NWs) are promising one-dimensional nanostructures with applications in nanoelectronic,[1] nanophotonic,[2] and nanosensing[3] devises. Fundamental studies of NW growth and physical properties are also of major interest. NW materials include elementary semiconductors Si and Ge, III–V, II–VI compounds and some oxides. Using modern epitaxy techniques, such as metal-organic chemical-vapor deposition (MOCVD) (Refs. 4–6) or molecular-beam epitaxy (MBE),[7–9] NWs with radii on the order of 10 nm and length up to tens of micrometers can be fabricated. NWs are usually obtained by the vapor-liquid-solid (VLS) mechanism[10] on the surfaces activated by the drops of a metal growth catalyst (e.g., Au). Due to the ability to accommodate strain in two dimensions, NW geometry is ideal for monolithic integration of semiconductor materials with different lattice constants, in particular, of III–V materials on silicon.[7,11,12] Geometrical and structural properties of NWs at given material system are determined by the size of seed drops and the deposition conditions. Ideally, NW would grow perpendicular to the (111) substrate surface at the position and with the radius dictated by the seed drop while the length would be proportional to the deposition time. This property is considered as one of the main advantages for the size, shape, and position controlled fabrication of NWs.[13] It is known, however, that many thermodynamic and kinetic growth effects impose certain limitations on the NW morphology as well as crystal structure [hexagonal wurtzite (WZ) or cubic zinc-blende (ZB) phase of III–V NWs (Refs. 9 and 12)].

Long ago, Givargizov and Chernov[14] discovered that wires would not grow smaller than a certain minimum radius (quantity on the order of few tens of nanometers in the case of Si wires deposited from vapors of $SiCl_4$ and H_2 on the Si(111) surface with Au catalyst at surface temperature ~1000 °C). They attributed the observed growth behavior to the Gibbs-Thomson (GT) effect of elevation of chemical potential in a wire with a cylindrically or prismatically curved surface. Later on, many works have been devoted to studying the growth properties of different NWs.[4,5,7–9,12,15–25] It is now generally recognized that NW formation is influenced by the direct impingement onto the drop surface,[5,12,14] the adatom diffusion,[4,5,7–9,15,17,21,22,26] and the nucleation.[19,20,22,26–28] All these processes must be considered under the constraint of finite size of the drop and the growing NW. In stationary growth mode with a constant radius, the vertical growth rate is directly proportional to the number of semiconductor particles transferred to the drop via different kinetic pathways.[26] As follows from early theories of diffusion-induced growth (see Ref. 29 and references herein) as well as from more comprehensive diffusion models,[8,17,21] the NW growth rate is generally a function of its length. Therefore, the time dependence of NW length is nonlinear. Examples of some nonlinear curves can be found, for example, in Ref. 8. By neglecting the GT effect, the models of Refs. 8, 15, 17, and 21 predict all NWs growing infinitely at a time-dependent rate. In contrast, the models of Refs. 5, 22, and 23 (accounting for the GT effect) lead to the NWs growing infinitely at a time-independent rate, provided that their radius is larger than the minimum.

The first aim of this paper is to show that the general growth behavior is much more complex. We present and analyze the exact solution to the kinetic equation of stationary NW growth that is equally applicable to MOCVD, MBE, and other deposition techniques. The exact solution for the NW length contains contributions from the diffusion of surface and sidewall adatoms. Due to the GT effect and different activities of semiconductor materials in different phases, each of these contributions could be of either signs. This allows for different growth scenarios, depending on the

deposition conditions, the radius, and the initial length of a NW. In the diffusion-induced mode, four modes are possible: (I) infinite growth; (II) decomposition (negative growth); (III) restricted growth leading to a finite length; and (IV) continuing growth such that NWs with larger initial length grow infinitely and NWs with smaller initial length evaporate. Among these, only the conventional mode (I) has been considered in the literature[4,5,7,8,15–23,30] while nontrivial scenarios (II)–(IV), to the best of our knowledge, have not been discussed earlier. We will also present an experimental evidence of scenarios (II) and (IV) in Au-assisted MBE of GaAs NWs.

The second objective of the paper is the control of crystal phase of GaAs NWs by using the intelligent manipulation with the NW structure in the growth scenario (IV), where a low-temperature growth is followed by a high-temperature deposition. It is well known that, in contrast to their cubic ZB phase under bulk form, GaAs and other III–V NWs often adopt hexagonal WZ structure.[6,9,12,22,27,28,30–35] In many cases, the structure of NWs is not stable and exhibits a spontaneous switching between different phases, creating rotational twins and stacking faults.[27,31,32,36] This clearly impedes material properties so the control over the phase purity is now considered as one of the main challenges in III–V NW technology. Generally, the prevalence of WZ structure requires sufficiently small radius[12,33,35] and high supersaturation in a liquid drop[27] while ZB NWs are formed at larger radius and lower supersaturation. Recently, a method has been proposed to obtain the stacking-fault-free ZB GaAs NWs by minimizing supersaturation during MBE [particularly, by using the high-index (311)B substrates].[36] However, for practical applications it is important to control the crystal structure of sufficiently thin straight NWs that are perpendicular to the substrate. In MBE case, lower supersaturation relates to a higher surface temperature,[22] where the NWs cannot be obtained by the standard VLS procedure [for GaAs NWs on the GaAs(111)B, the upper temperature limit of Au-assisted MBE amounts to 600 °C (Ref. 37)]. We will demonstrate that the MBE growth on the pre-existing low-temperature NW seeds of a short length can be performed at 630 °C and that the high-temperature section of GaAs NW is pure ZB for the radii of only 15–20 nm.

II. THEORETICAL MODEL

Stationary growth model, discussed in more detail in Ref. 23, is schematized in Fig. 1. We consider a single cylindrical NW with the uniform radius R and the contact angle of spherical drop β. Nonstationary growth effects[26] and the lateral growth[31] are not taken into account. Impinging flux is defined by the effective arrival rate J and the incident angle α. The latter equals the incident angle of molecular beam in MBE. In MOCVD, we formally put $\sin\alpha=\cos\alpha=\tan\alpha \equiv 1$ since vapors entirely surround the drop and the NW. Deposition rate is given by $V=J\Omega_s\cos\alpha$, with Ω_s as the elementary volume in the solid phase. Drop surface in contact with the vapor is characterized by the surface energy γ. The drop can be either liquid [(VLS mechanism)[10]] or solid (vapor-solid-solid mechanism[30]); below we refer to most

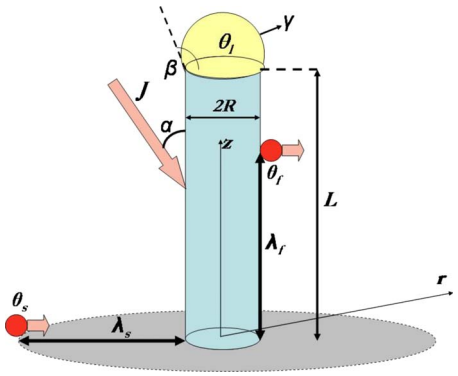

FIG. 1. (Color online) Illustration of the NW growth model with the parameters described in the text.

common VLS case. The NW temperature across its length and the drop temperature are assumed as being equal to the surface temperature T. In order to account for different precursor decomposition rates at different surfaces in the case of MOCVD, we introduce the temperature-dependent pyrolysis efficiencies at the liquid (χ_l), substrate (χ_s), and sidewall (χ_f) surfaces.

Stationary adatom concentrations on the substrate surface (n_s) and sidewall facets (n_f) obey diffusion equations

$$D_s\Delta n_s + \chi_s J\cos\alpha - \frac{n_s}{\tau_s} = 0, \tag{1}$$

$$D_f\frac{d^2n_f}{dz^2} + \omega\chi_f J\sin\alpha - \frac{n_f}{\tau_f} = 0. \tag{2}$$

Here, Δ is the two-dimensional (2D) Laplace operator in the substrate plane (r), z is the vertical coordinate, D_s and D_f are the diffusion coefficients, and τ_s and τ_f are the effective lifetimes on the substrate and the sidewalls, respectively. Numerical values of τ_s and τ_f are limited by the desorption from the surface or by the nucleation. The coefficient ω in Eq. (2) equals 1 in MOCVD and $1/\pi$ in MBE. Four boundary conditions to Eqs. (1) and (2), given in Ref. 23, require constant adatom concentration on the surface far away from the NW, the continuity of chemical potential at the NW base and top, and the continuity of diffusion flux at the NW base.

Following the procedure of Ref. 23, the diffusion-induced contribution to the growth rate is obtained from the exact solutions of Eqs. (1) and (2). The result can be presented in the form

$$\left(\frac{dL}{dH}\right)_{diff} = \frac{BU(L/\lambda_f)+C}{U'(L/\lambda_f)}, \tag{3}$$

where L is the NW length, $H=Vt$ is the deposition thickness, t is the time, and $\lambda_f=\sqrt{D_f\tau_f}$ is the diffusion length on the sidewalls. The R-dependent coefficients B and C are defined as follows:

$$B = \chi_f \omega \frac{2\lambda_f \tan\alpha}{R}\left(1 - \frac{\theta_l}{\theta_f}\right), \quad C = \chi_s \frac{2\lambda_s}{R}\delta(R/\lambda_s)\left(1 - \frac{\theta_l}{\theta_s}\right). \tag{4}$$

The functions $U(l)$ and $U'(l)$ in Eq. (4) are given by

$$U(l) = \sinh(l) + \nu\delta(R/\lambda_s)[\cosh(l) - 1],$$

$$U'(l) \equiv \frac{dU}{dl} = \cosh(l) + \nu\delta(R/\lambda_s)\sinh(l). \tag{5}$$

Here, $\lambda_s = \sqrt{D_s \tau_s}$ is the effective diffusion length on the substrate surface, $\delta(R/\lambda_s) = K_1(R/\lambda_s)/K_0(R/\lambda_s)$, K_i are the modified Bessel function of the second kind of order i and $\nu = (D_s \lambda_f \sigma_f / D_f \lambda_s \sigma_s)$. The quantities $\theta_s = \chi_s J \tau_s \sigma_s \cos\alpha$ and $\theta_f = \omega \chi_f J \tau_f \sigma_f \sin\alpha$ denote the maximum coverage of the surface by the substrate and the sidewalls adatoms, respectively, with σ_s and σ_f as the areas of corresponding adsorption sites. The R-dependent activity of semiconductor material in the drop is defined as $\theta_l = \exp(\mu_l^\infty / k_B T + R_{GT}/R)$, where μ_l^∞ is the chemical potential in the infinite liquid phase, $R_{GT} = (2\gamma\Omega_l \sin\beta)/(k_B T)$ is the characteristic GT radius, Ω_l is the elementary volume in the liquid, and k_B is the Boltzmann constant.[22] Coefficient B describes the sidewall adatoms and coefficient C stands for the substrate adatoms. Corresponding diffusion fluxes are positive when the activity of adatoms is larger than the liquid activity and negative otherwise.

NW growth rate is also influenced by the adsorption-desorption processes on the drop surface[4,5,12,20] and by the growth of quasi-2D layer on the substrate surface (S).[7,8,22,23] These contributions can be collected in one term, $(dL/dH)_{ADS} = A$. Here, A is a certain L-independent function of NW radius R, which can also be of either signs due to the GT effect. The explicit expression for A, which can be found in Ref. 38, depends on the epitaxy technique (MBE or MOCVD) and is omitted here as inessential for further analysis. Overall growth rate is given by $dL/dH = (dL/dH)_{diff} + (dL/dH)_{ADS}$. Introducing the normalized length, $l \equiv L/\lambda_f$, and the deposition thickness, $h \equiv H/\lambda_f$, the equation for NW length writes

$$\frac{dl}{dh} = \frac{BU(l) + C}{U'(l)} + A, \quad l(h=0) = l_0. \tag{6}$$

The initial condition at $h=0$ determines the length l_0 of pre-existing NWs, e.g., obtained at different growth conditions.

Nonlinear differential Eq. (6) with function $U(l)$ given by Eq. (5) can be integrated analytically at arbitrary coefficients A, B, and C and initial condition l_0. The result is obtained in the form of reverse dependence $h(l)$,

$$h(l) = \frac{1}{B^2 - A^2}\left\{B \ln\left[\frac{F(l)}{F(l_0)}\right] - A(l - l_0)\right\} + A[\Psi(l) - \Psi(l_0)]. \tag{7}$$

The functions $F(l)$ and $\Psi(l)$ in Eq. (7) are determined by

$$F(l) = (A + B\nu\delta)[\cosh(l) - 1] + (B + A\nu\delta)\sinh(l) + A + C, \tag{8}$$

$$\Psi(l) = \frac{2(C - B\nu\delta)}{(B^2 - A^2)\sqrt{G}} \times \arctan\left[\frac{(A - C + 2B\nu\delta)\tanh(l/2) + B + A\nu\delta}{\sqrt{G}}\right], \tag{9}$$

where $G = A^2[1 - (\nu\delta)^2] - B^2 - C^2 + 2BC\nu\delta$.

Kinetic Eq. (6) takes a very simple form in the limit case of $A \to 0$ [diffusion-induced growth with $\lambda_s/R \gg 1$, $(\lambda_f/R)\tan\alpha \gg 1$].[7,8,21] Introduction of a new variable U converts Eq. (6) at $A=0$ to

$$\frac{dU}{dh} = BU + C, \quad U(h=0) = U(l_0). \tag{10}$$

Solution to Eq. (10) is given by

$$h(l) = \frac{1}{B}\ln\left[\frac{BU(l) + C}{BU(l_0) + C}\right], \tag{11}$$

where $U(l)$, by definition, increases with l and equals zero at $l=0$.

The aim of next section is to consider possible growth modes of NWs following from the obtained solutions. We show that the time evolution of NW length will generally depend on the sign of kinetic coefficients and the initial length l_0. The analysis will be illustrated by some numerical examples in the case of Au-assisted MBE of GaAs NWs on the GaAs(111)B substrate.

III. GROWTH SCENARIOS

The first general property of Eq. (6) is the following. Since $U(0)=0$, $U'(0)=1$, and $U(l) \sim U'(l) \sim \exp(l)$ at $l \to \infty$, Eq. (6) becomes linear in l in two important particular cases,

$$\left(\frac{dl}{dh}\right)_{l\to 0} = C + A, \quad \left(\frac{dl}{dh}\right)_{l\to\infty} = B + A. \tag{12}$$

The first Eq. (12) shows that at the beginning of growth the NW is fed from the substrate and through the drop. This result has been obtained earlier in Refs. 5, 21, and 22. The second relationship demonstrates that tall NWs are fed only from the sidewalls and through the drop since the surface adatoms evaporate before they reach the NW top. The condition of NW formation from $l_0=0$ (drop lying on the substrate surface) yields $C+A>0$ while the infinite growth at $l \to \infty$ is possible at $B+A>0$. At $A \to 0$, these conditions are reduced to $C>0$ and $B>0$, respectively.

We now analyze possible scenarios of NW growth following from simplified Eq. (10) in the diffusion-induced mode. Obviously, the sign of the right-hand side of Eq. (10) determines the sign of derivative dl/dh; the NW growth rate is positive at $BU+C>0$ and negative at $BU+C<0$. The points where $BU(l_*)+C=0$ are the stationary points with corresponding critical lengths l_*. Four possible behaviors of the linear function with sign alternating coefficients B and C are presented in Fig. 2, where the arrows indicate the time evolution of nonlinear system considered. We therefore arrive at

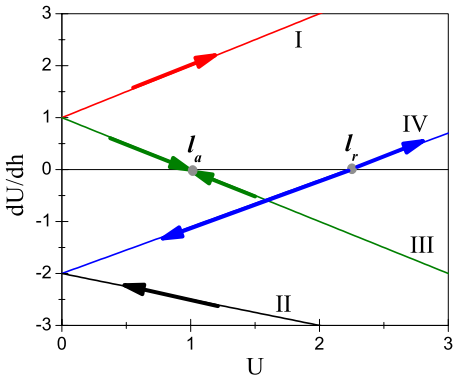

FIG. 2. (Color online) Illustration of the growth modes described in the text: I—infinite growth, II—negative growth, III—averaging growth with attractive stationary point $l_*=l_a$, and IV—continuing growth with repulsive stationary point $l_*=l_r$.

four possible growth scenarios: (I) $B>0$, $C>0$: NW of any initial length l_0 grows infinitely. (II) $B<0$, $C<0$: NW of any initial length l_0 decay. (III) $B<0$, $C>0$: critical length determined by $U(l_*)=C/|B|$ is the attractive stationary point such that the NWs with initial length $l_0<l_*$ grow to l_* and the NWs with $l_0>l_*$ diminish their length to l_* (averaging growth). (IV) $B>0$, $C<0$: critical length determined by $U(l_*)=|C|/B$ is the repulsive stationary point such that the NWs with initial length $l_0<l_*$ decay and the NWs with $l_0>l_*$ grow infinitely (continuing growth).

Since U, C, and B are the functions of R, the growth scenario at given deposition conditions would generally depend on the radius of a particular NW. Equations (4) for B and C in view of the above definition for the liquid activity take the form

$$B=\chi_f\omega\frac{2\lambda_f}{R}\tan\alpha\left[1-\frac{\exp(R_{GT}/R)}{\theta_{fl}}\right],$$

$$C=\chi_s\frac{2\lambda_s}{R}\delta(R/\lambda_s)\left[1-\frac{\exp(R_{GT}/R)}{\theta_{sl}}\right]. \quad (13)$$

Here, $\theta_{fl}\equiv\theta_f/\theta_l^\infty$ and $\theta_{sl}\equiv\theta_s/\theta_l^\infty$ are the effective supersaturations of sidewall and surface adatoms with respect to the infinite liquid alloy with activity $\theta_l^\infty=\exp(\mu_l^\infty/k_BT)$. Obviously, coefficients B and C change sign at critical radii R_B and R_C determined by

$$R_B=\frac{R_{GT}}{\ln\theta_{fl}},\quad R_C=\frac{R_{GT}}{\ln\theta_{sl}}. \quad (14)$$

Diffusion flux of surface adatoms is positive at $R>R_C$ and negative at $R<R_C$; the condition for the NW growth from zero length is $R>R_C$. In this sense, critical radius R_C is equivalent to the Givargizov-Chernov minimum radius below which the NWs would not nucleate, although the expression for R_C is different from the result of Ref. 14. Diffusion flux of sidewall adatoms is positive at $R>R_B$ and negative at $R<R_B$; the infinite growth at $l\to\infty$ yields $R>R_B$. Four growth modes of NWs can be therefore reformulated in terms of their radius: (I) infinite growth at $R>\max(R_B,R_C)$; (II) negative growth at $R<\min(R_B,R_C)$; (III) averaging growth at $R_C<R<R_B$; (IV) continuing growth at $R_B<R<R_C$.

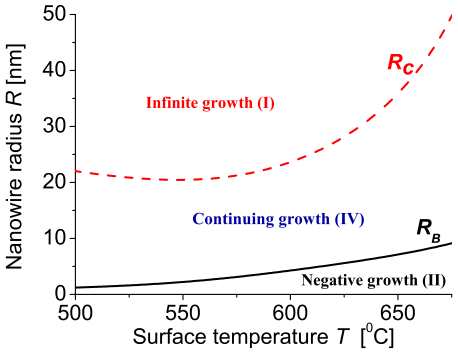

FIG. 3. (Color online) Typical growth diagram of Au-assisted MBE of GaAs NWs for the model parameters described in the text: zone I—infinite growth, zone IV—continuing growth, and zone II—negative growth.

To be more specific, consider the case of Au-assisted MBE ($\chi_s=\chi_f=1$ and $\omega=1/\pi$) of GaAs NWs on the GaAs(111)B surface. We study the temperature dependences of R_B and R_C given by Eq. (14) with $\theta_{fl}=(1/\pi)(V/h)(\sigma_f/\sigma_s)\tau_f\tan\alpha\exp(-\mu_l^\infty/k_BT)$ and $\theta_{sl}=(V/h)\tau_s\exp(-\mu_l^\infty/k_BT)$. Here, V/h is the equivalent deposition rate in monolayers (MLs) per second, for which we use the typical value of 1 ML/s.[8] The ratio σ_f/σ_s amounts to $4/\sqrt{6}$ for the (110) sidewall and (111)B substrate surfaces of ZB GaAs. The adatom lifetime on the sidewalls, limited by the desorption, is as usual taken in the Arrhenius form $\tau_f=\nu_f^{-1}\exp(E_A^f/k_BT)$. We use the values of $E_A^f=2$ eV for the activation energy for desorption (estimated from the data of Ref. 39) and $\nu_f=10^{11}$ s^{-1} for the corresponding vibration frequency. As mentioned above, the adatom lifetime on the substrate is limited either by the desorption (at high temperatures) or by the surface nucleation (at low temperatures). As a result, τ_s has a maximum at a certain temperature.[22,40] We therefore utilize the model of Ref. 40 of the form $1/\tau_s=1/\tau_s^0+1/\tau_n$, with τ_s^0 as the lifetime of a single adatom at no growth conditions and τ_n as the effective nucleation time. The conventional Arrhenius temperature dependence $\tau_s^0=\nu_s^{-1}\exp(E_A^s/k_BT)$ is used at $E_A^s=1.64$ eV and $\nu_s=10^{10}$ s^{-1}, the values approximately corresponding to the MBE of GaAs on the GaAs(111)B substrate.[22] The temperature dependence of $\tau_n=\nu_n^{-1}\exp(-E_n/k_BT)$ with $E_n=0.97$ eV and $\nu_n=3\times10^{-5}$ s^{-1} is taken from Ref. 22. Since nothing can be said about the value of $\mu_l^\infty(T)$, we can only use the estimates of Ref. 22, lying within the thermodynamically permitted range of liquid chemical potential during the growth. Finally, the value of $R_{GT}=6.6$ nm corresponds to 40% concentration of Ga in the Au-Ga alloy [with surface energy $\gamma=0.72$ J/m^2 for pure liquid Ga and 1.14 J/m^2 for pure liquid Au (Ref. 41)] and the contact angle $\beta=120°$.

Theoretical curves for $R_B(T)$ and $R_C(T)$ are presented in Fig. 3. The temperatures higher than 500 °C yield straight GaAs NWs with uniform radius from base to top,[37] for which the stationary growth model is directly applicable. As seen from Fig. 3, infinite growth of NWs [scenario (I)] cannot proceed at very high temperatures due to the negative

diffusion from the NW top to the substrate. For the model parameters considered, the averaging growth to a finite length [scenario (III)] is never observed since $R_C > R_B$ within the entire temperature domain. The NW growth is completely forbidden in zone II below the curve $R_B(T)$ [scenario (II)], which is, however, smaller than 10 nm for all reasonable temperatures. Nontrivial scenario (IV) of continuing growth can happen in zone IV between the curves $R_B(T)$ and $R_C(T)$, where the growth cannot proceed from the drop lying on the substrate surface but can continue from pre-existing NWs with sufficiently large initial length $l_0 > l_*$. Figure 3 shows that the domain of NW radii exhibiting such continuing growth extends at higher surface temperatures. As follows from the equation $U(l_*) = |C|/B$ and $U(l) \propto \exp(l)$ at $l \gg 1$, the temperature dependence of dimensional critical length L_* at high T mimics that of $\lambda_f(T)$ with minor logarithmic corrections. As the diffusion length $\lambda_f(T)$ decreases with T, the critical length for the continuing growth becomes smaller at higher T.

To conclude this section, we note that negative growth via scenario (II) during MBE or MOCVD should always take place at zero deposition rate ($J=0$), when the coefficients B and C become negative. Since the diffusion flux is directed from the NW top to the substrate, the decrease in NW length should be associated with the increase in surface layer thickness. It should be also mentioned that the growth scenarios in MOCVD technique strongly depend on the temperature behavior of precursor decomposition probabilities, $\chi_s(T)$ and $\chi_f(T)$, which may be different at the substrate and sidewall surfaces. The resulting growth diagram will therefore differ from the MBE case. This issue requires a separate study which will be presented elsewhere. Finally, the detailed analysis of general growth Eq. (6) at $A \neq 0$ leads to six possible growth scenarios instead of four so that nontrivial cases of continuing and averaging growth could be observed within certain intervals of NW radii.[38]

IV. EXPERIMENTAL EVIDENCE OF NEGATIVE AND CONTINUING GROWTH

Obviously, scenario (I) corresponds to most of the growth experiments reported in the literature.[4,7–9,15,21,24,25] We found experimental evidences of scenarios (II) and (IV) in the case of Au-assisted MBE of GaAs NWs on the GaAs(111)B substrates. In our growth experiments in Riber 32 MBE setup, substrate was deoxidized at 620 °C and a GaAs buffer layer was grown at 630 °C. A 70 nm AlGaAs marker layer was systematically inserted in this buffer layer in order to have an absolute reference of vertical coordinate z. Then the substrate temperature was decreased and stabilized to the value desired for the NW growth. An amount of Au equivalent to a uniform layer of 1 nm was deposited on the substrate surface from an Au source installed in the MBE growth chamber. This procedure resulted in the formation of Au droplets alloyed with the substrate constituents which could activate the NW growth.

Negative growth is well illustrated by our annealing experiments. GaAs NWs were grown at 530 °C for 15 min with an As_4 beam equivalent pressure of 6×10^{-6} Torr and a Ga flux corresponding to a nominal growth rate V of 0.2 nm/s. This growth stage produced NWs of 800 nm length and 25 nm diameter in average, as shown in Fig. 4(a). Several samples were grown and subsequently annealed in the growth chamber under the As_4 flux at 630 °C and for various durations. After the growth, the resulting morphology of NW ensembles was investigated by scanning electron microscopy (SEM). The sample cross sections were observed after cleaving and the contrast between GaAs and AlGaAs allowed us to locate the marker layer and then to determine the exact position where Au was deposited before initiating the NW growth. We could deduce the thickness of the 2D GaAs layer growing concomitantly with the NWs. The results are presented in Figs. 4(b) and 4(c). It is obvious from this figure that NWs gradually decompose during the annealing. We also observed that the average thickness of GaAs 2D layer increased from 110 nm for nonannealed samples to 147 nm and 176 nm for 4 and 5 min annealing time. This clearly indicates that the NW decomposition did not result from reevaporation of Ga which is not expected at 630 °C. We propose the following mechanism: NWs dissolve in the catalyst droplets, As is most likely re-evaporated from the drop but Ga migrates from the droplet to the surface where it can reincorporate the GaAs solid phase since As_4 flux is supplied. In other words, we observe the negative NW growth rate at $V=0$ which is predicted in scenario (II) where adatom diffusion flow is reversed as compared to the standard situation of scenario (I).

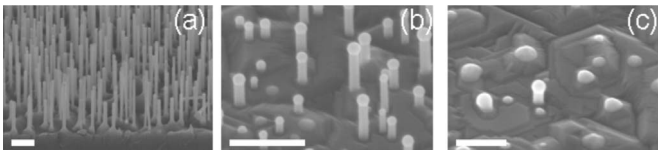

FIG. 4. GaAs NWs after *in situ* anneal under As_4: (a) reference sample without annealing; (b) 4 min anneal; (c) 5 min anneal. Scale bars represent 200 nm.

Another series of MBE growth experiments evidence that continuing growth via scenario (IV) also happens. Au catalyst was deposited on GaAs(111)B with the same procedure as described hereinabove. After Au deposition, we tried to grow GaAs NWs with the following conditions: in a first sample (sample A) the growth was realized at 630 °C for 15 min. The SEM view shown in Fig. 5(a) reveals that NWs do not grow at this relatively high temperature and the segregation of the Au particles at the substrate surface is observed.

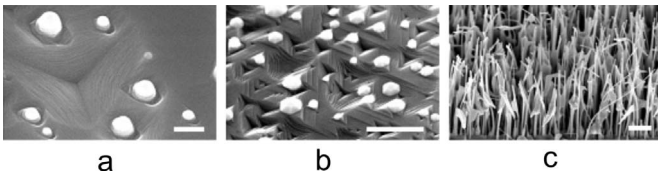

FIG. 5. Samples of GaAs grown with a low-temperature (530 °C) step of variable duration t_{LT}, followed by a high-temperature step (630 °C) of 15 min. (a) sample A with $t_{LT}=0$; (b) sample B with $t_{LT}=1.5$ min; (c) sample C with $t_{LT}=15$ min. Scale bar is 400 nm.

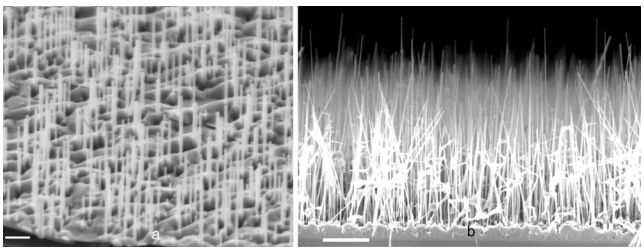

FIG. 6. SEM cross views of GaAs NWs grown with a low-temperature step for $t_{LT}=12$ min (a) before and (b) after the high-temperature growth. Scale bars are 200 nm in Fig. 6(a) and 2 μm in Fig. 6(b).

We have previously reported similar results.[37] Then, two other samples were grown by using a two-temperature process: the first growth step was performed at 530 °C for $t_{LT}=1.5$ min (sample B) or 15 min (sample C). At this temperature, NWs are formed, as already observed in Fig. 4(a). After this first step, the temperature was ramped to 630 °C within 2 min. During this ramping, the incident Ga and As_4 fluxes were maintained. Finally the growth was continued at 630 °C for 15 min for sample B and C. Therefore, this last growth step was similar for the three samples A, B, and C. Figures 5(b) and 5(c) show SEM images of samples B and C. It is observed that no NWs are present in sample B, the final figure being quite comparable to sample A. This means that the NWs formed at the low-temperature-growth step of 1.5 min, did not continue to grow at high T; either they were decomposed like in annealing experiments or were buried by GaAs growing faster on the rest of the surface. On the contrary, sample C shows NWs longer than what is expected for the 15 min of growth at low temperature; most of the NWs are longer than 2 μm [Fig. 5(c)]. Obviously, in this sample, NW growth was possible at high T. Scenario (IV) is believed to be responsible for the different behaviors of samples B and C; the initial NW length is lower (sample B) or higher (sample C) than the critical length. The latter corresponds to the NW sidewall cross section which intercepts enough incoming Ga flux to compensate for the flow of adatoms which otherwise diffuses from the drop to the substrate surface, leading to NW decomposition.

GaAs NWs shown in Fig. 5(c) have rather complex geometry; some of them develop branches and the majority of NWs are tapered toward their top. Such complex geometry can be explained by changes in drop size and position at

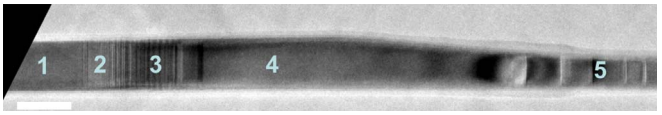

FIG. 7. (Color online) TEM image of a NW grown with two-temperature steps (detached from sample C of Fig. 5) showing phase transitions along the NW length. From left to right: pure WZ phase corresponding to 530 °C growth (1), WZ with twins (2) and highly faulted WZ/ZB mix up (3) corresponding to temperature ramping, pure ZB phase corresponding to 630 °C (4), significant reduction in the diameter followed by phase mixing (5). Scale bar represents 40 nm.

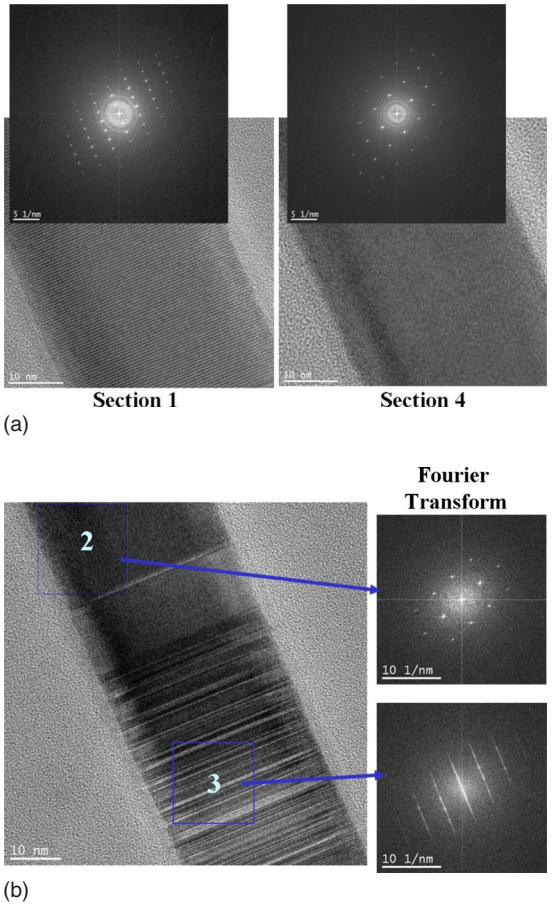

FIG. 8. (Color online) (a) High-resolution TEM closeups of pure WZ (section 1 of Fig. 7) and ZB (section 4) GaAs NW; (b) enlarged TEM images of WZ with stacking faults (section 2) and highly faulted WZ/ZB mix up (section 3). Inserts show the corresponding Fourier transforms.

elevated temperature. Most probably, the drop first inflates with the temperature and then becomes unstable on the NW top so that it splits into several smaller drops. Some of those give branches and other may migrate to the substrate. We note that similar MBE growth experiments carried out in EP1203 setup at slightly different conditions allowed us to obtain more regular shape of NWs. The GaAs(111)B surfaces were activated by Au with the same procedure as described above. A low-temperature growth was performed at $T=550$ °C form atomic Ga and As_4 beams with a nominal growth rate of 0.3 nm/s for $t_{LT}=1$, 2, and 12 min. After the temperature ramping to 630 °C, the high-temperature-growth step was performed at a lower nominal growth rate of 0.15 nm/s for 48 min. Similarly to the previous case, NWs with $t_{LT}=1$ and 2 min did not grow. NWs with $t_{LT}=12$ min, having average initial length of 800 nm [Fig. 6(a)] continued to grow at $T=630$ °C and reached more than 10 μm in length [Fig. 6(b)] after this high-temperature step.

V. CONTROL OF CRYSTAL PHASE

An interesting feature is the impact of the high-temperature growth on the crystal structure of GaAs NWs.

As already discussed in Sec. I, most of III–V NWs grown by different deposition techniques form in the high-pressure WZ phase.[6,9,12,30–32] This surprising effect is observed only for NWs and never happens in a bulk III–V materials, 2D layers and even in quantum dots obtained at ambient pressure. In the case of GaAs, the difference of bulk cohesive energies between WZ and ZB phase amounts to 16.6 meV per GaAs pair.[42] To overcome this difference and to obtain WZ GaAs under the bulk form, one should apply a huge pressure >100 GPa.[43] Theoretical models of WZ phase formation in III–V NWs developed so far attributed the observed effect to a decrease in lateral surface energy in WZ NWs (Refs. 12, 27, and 33–35) due to a lower number of dangling bonds on the sidewalls or the edges separating the latter. It was argued that the contribution from the surface energy to the overall free enthalpy of NW formation diminishes with increasing the NW radius. Therefore, the surface energy gain outweighs the difference in bulk cohesive energies only in sufficiently thin NWs. Equilibrium considerations result in the critical radius of ZB to WZ phase transition smaller than 10 nm in the case of GaAs NWs.[33,35] However, many experimental results show that GaAs NWs of radii several times larger that this critical value, still adopt the WZ structure.[9,27,36,44] This is because the models of Refs. 33 and 35 consider the energy balance of fully formed NWs of defined geometry and ignore the nucleation stage. More realistically, it has been proposed that the critical parameter is the size of the nuclei formed at the catalyst/NW interface during the NW growth.[27] This size is inversely proportional to the supersaturation in the liquid. This model was supported by experimental results[27,44] showing that ZB phase is systematically observed during transient growth steps in the beginning and in the end of deposition during which the supersaturation in the liquid is less than during the steady NW growth (where the crystal structure is predominantly WZ). As suggested in Ref. 27 and further developed in Refs. 22 and 28, crystal structure of NWs is strongly affected by mononuclear nucleation at the triple line; growth at high supersaturation (small nuclei with prevalence of their edge energy) should onset the formation of WZ phase while the low supersaturation (larger nuclei with prevalence of their cohesive energy) conditions should lead to the prevalence of ZB structure. Since in MBE case the supersaturation generally decreases with increasing the surface temperature,[22] a high-temperature growth via scenario (IV) could provide a method for the production of stacking-fault-free ZB NWs of sufficiently small radii, which is of paramount importance for applications.

High-resolution transmission electron microscopy (TEM) images of a NW of 37 nm diameter in the bottom part, detached from sample C of Fig. 5, are shown in Fig. 7. Figure 8 presents the enlarged TEM images of four sections of NW shown in Fig. 7 and the corresponding Fourier transforms of the real-space images. The bottom part of the NW [section 1 in Figs. 7 and 8(a)] corresponds to the low-temperature growth and it has pure WZ structure, as seen from the TEM image of section 1 and the corresponding Fourier transform in Fig. 8(a). Then, the WZ structure presents an increasing number of stacking faults in a region which corresponds to the temperature ramping, where the supersaturation starts to decrease [section 2 in Figs. 7 and 8(b)]. At the end of this region, the crystal structure switches to ZB structure with a few twins. Finally, a 200 nm segment of pure ZB is found [section 4 in Figs. 7 and 8(a)], as demonstrated by the TEM image and the corresponding Fourier transform in Fig. 8(a). In this ZB segment, the NW diameter first increases slightly and then reduces significantly. These changes in diameter are most likely following the changes in catalyst drop size discussed hereinabove; inflation of the drop with temperature as it fills with more Ga; splitting the drop or loss of its constituents when mechanical instability is attained. Below 25 nm diameter, stacking faults and phase mixing reappear (section 5 in Fig. 7). This latter observation is not clearly understood at the moment but it seems to be a consequence of the smaller radius of the NW and larger relative contribution from the surface energy, as discussed hereinabove. These results qualitatively support previous theoretical findings[22,27,28] and demonstrates that GaAs NWs grown at 630 °C by the two-step procedure of scenario (IV) have pure ZB phase.

To conclude, we have developed nonlinear model of NW formation and have shown that in the diffusion-induced mode there are four possible scenarios of NW growth: (I) positive, (II) negative, (III) averaging, and (IV) continuing growth. Theoretical growth diagram in the case of Au-assisted MBE of GaAs NWs separates the domains of scenarios (I) and (IV) in (II) in (T,R) plane while the observation of scenario (III) is unlikely. Theoretical predictions are in qualitative agreement with our experimental results which validate nontrivial growth modes (II) and (IV). We have demonstrated that the two-step growth with the temperature ramping could provide a method to obtain pure ZB sections in III–V NWs at high growth temperatures (relating to a low supersaturation in the liquid phase). In particular, two-step MBE growth via scenario (IV) enables to obtain stacking-fault-free ZB GaAs NWs of only 15–20 nm radii, which would not be possible by the standard VLS growth procedure at constant temperature.

ACKNOWLEDGMENTS

This work was partially supported by the Russian Federal Agency for Science and Innovation, the SANDIE Network of Excellence of the European Commission, different grants of Russian Academy of Sciences and Russian Foundation for Basic Research.

*dubrovskii@mail.ioffe.ru

[1] T. Bryllert, L. E. Wernersson, T. Lowgren, and L. Samuelson, Nanotechnology **17**, S227 (2006).
[2] S. Gradecak, F. Qian, Y. Li, H. G. Park, and C. M. Lieber, Appl. Phys. Lett. **87**, 173111 (2005).
[3] F. Patolsky, G. Zheng, and C. M. Lieber, Nanomedicine **1**, 51 (2006).
[4] W. Seifert, M. Borgstrom, K. Deppert, K. A. Dick, J. Johansson, M. W. Larsson, T. Martensson, N. Skold, C. P. T. Svensson, B. A. Wacaser, L. R. Wallenberg, and L. Samuelson, J. Cryst. Growth **272**, 211 (2004).
[5] L. E. Fröberg, W. Seifert, and J. Johansson, Phys. Rev. B **76**, 153401 (2007).
[6] L. C. Chuang, M. Moewe, S. Crankshaw, C. Chase, N. P. Kobayashi, and C. Chang-Hasnain, Appl. Phys. Lett. **90**, 043115 (2007).
[7] L. Schubert, P. Werner, N. D. Zakharov, G. Gerth, F. M. Kolb, L. Long, U. Gösele, and T. Y. Tan, Appl. Phys. Lett. **84**, 4968 (2004).
[8] V. G. Dubrovskii, G. E. Cirlin, I. P. Soshnikov, A. A. Tonkikh, N. V. Sibirev, Yu. B. Samsonenko, and V. M. Ustinov, Phys. Rev. B **71**, 205325 (2005).
[9] J. C. Harmand, G. Patriarche, N. Péré-Laperne, M.-N. Mérat-Combes, L. Travers, and F. Glas, Appl. Phys. Lett. **87**, 203101 (2005).
[10] R. S. Wagner and W. C. Ellis, Appl. Phys. Lett. **4**, 89 (1964).
[11] F. Glas, Phys. Rev. B **74**, 121302(R) (2006).
[12] M. Moewe, L. C. Chuang, V. G. Dubrovskii, and C. Chang-Hasnain, J. Appl. Phys. **104**, 044313 (2008).
[13] B. J. Ohlsson, M. T. Björk, M. H. Magnusson, K. Deppert, and L. Samuelson, Appl. Phys. Lett. **79**, 3335 (2001).
[14] E. I. Givargizov and A. A. Chernov, Kristallografiya **18**, 147 (1973).
[15] J. Johansson, C. P. T. Svensson, T. Mårtensson, L. Samuelson, and W. Seifert, J. Phys. Chem. B **109**, 13567 (2005).
[16] I. Avramov, Nanoscale Res. Lett. **2**, 235 (2007).
[17] G E. Cirlin, V. G. Dubrovskii, N. V. Sibirev, I. P. Soshnikov, Yu. B. Samsonenko, A. A. Tonkikh, and V. M. Ustinov, Semiconductors **39**, 557 (2005).
[18] A. A. Golovin, S. H. Davis, and P. W. Voorhees, J. Appl. Phys. **104**, 074301 (2008).
[19] D. Kashchiev, Cryst. Growth Des. **6**, 1154 (2006).
[20] V. G. Dubrovskii and N. V. Sibirev, Phys. Rev. E **70**, 031604 (2004).
[21] V. G. Dubrovskii, N. V. Sibirev, R. A. Suris, G. E. Cirlin, V. M. Ustinov, M. Tchernysheva, and J. C. Harmand, Semiconductors **40**, 1075 (2006).
[22] V. G. Dubrovskii, N. V. Sibirev, J. C. Harmand, and F. Glas, Phys. Rev. B **78**, 235301 (2008).
[23] V. G. Dubrovskii, N. V. Sibirev, G. E. Cirlin, I. P. Soshnikov, W. Chen, R. Larde, E. Cadel, P. Pareige, T. Xu, B. Grandidier, J.-P. Nys, D. Stievenard, M. Moewe, L. C. Chuang, and C. Chang-Hasnain, Phys. Rev. B **79**, 205316 (2009).
[24] M. N. Jung, J. E. Koo, S. J. Oh, B. W. Lee, W. J. Lee, S. H. Ha, Y. R. Cho, and J. H. Chang, Appl. Phys. Lett. **94**, 041906 (2009).
[25] J. Sadowski, P. Dłużewski, S. Kret, E. Janik, E. Łusakowska, J. Kanski, A. Presz, F. Terki, S. Charar, and D. Tang, Nano Lett. **7**, 2724 (2007).
[26] V. G. Dubrovskii, N. V. Sibirev, G. E. Cirlin, J. C. Harmand, and V. M. Ustinov, Phys. Rev. E **73**, 021603 (2006).
[27] F. Glas, J. C. Harmand, and G. Patriarche, Phys. Rev. Lett. **99**, 146101 (2007).
[28] J. Johansson, L. S. Karlsson, K. A. Dick, J. Bolinsson, B. A. Wacaser, K. Deppert, and L. Samuelson, Cryst. Growth Des. **9**, 766 (2009).
[29] E. I. Givargizov, *Highly Anisotropic Crystals* (Springer, Berlin, 1987).
[30] K. A. Dick, K. Deppert, T. Martensson, S. Mandl, L. Samuelson, and W. Seifert, Nano Lett. **5**, 761 (2005).
[31] M. Tchernycheva, L. Travers, G. Patriarche, F. Glas, J. C. Harmand, G. E. Cirlin, and V. G. Dubrovskii, J. Appl. Phys. **102**, 094313 (2007).
[32] A. I. Persson, M. W. Larsson, S. Stengstrom, B. J. Ohlsson, L. Samuelson, and L. R. Wallenberg, Nature Mater. **3**, 677 (2004).
[33] T. Akiyama, K. Sano, K. Nakamura, and T. Ito, Jpn. J. Appl. Phys., Part I **45**, L275 (2006).
[34] M. Galicka, M. Bukala, R. Buczko, and P. Kacman, J. Phys.: Condens. Matter **20**, 454226 (2008).
[35] V. G. Dubrovskii and N. V. Sibirev, Phys. Rev. B **77**, 035414 (2008).
[36] H. Shtrikman, R. Popovitz-Biro, A. Kretinin, L. Houben, M. Heiblum, M. Bukala, M. Galicka, R. Buczko, and P. Kacman, Nano Lett. **9**, 1506 (2009).
[37] J. C. Harmand, M. Tchernycheva, G. Patriarche, L. Travers, F. Glas, and G. Cirlin, J. Cryst. Growth **301-302**, 853 (2007).
[38] V. G. Dubrovskii, N. V. Sibirev, and M. A. Timofeeva, Semiconductors **43**, 1226 (2009).
[39] M. Lopez and Y. Nomura, J. Cryst. Growth **150**, 68 (1995).
[40] V. G. Dubrovskii and N. V. Sibirev, J. Cryst. Growth **304**, 504 (2007).
[41] A. Zangwill, *Physics At Surfaces* (Cambridge University Press, Cambridge, 1988).
[42] C.-Y. Yeh, Z. W. Lu, S. Froyen, and A. Zunger, Phys. Rev. B **46**, 10086 (1992).
[43] M. I. McMahon and R. J. Nelmes, Phys. Rev. Lett. **95**, 215505 (2005).
[44] I. P. Soshnikov, G. E. Cirlin, A. A. Tonkikh, Y. B. Samsonenko, V. G. Dubrovskii, V. M. Ustinov, O. M. Gorbenko, D. Litvinov, and D. Gerthsen, Phys. Solid State **47**, 2213 (2005).